J Therm Spray Tech (2018) 27:1532–1541
https://doi.org/10.1007/s11666-018-0788-x

PEER REVIEWED

Hollow Plasma-Sprayed Spherical Nanostructured Titania Feedstock for Photocatalytic Applications

Xiaoyan He[1,2] · Kun Ren[1] · Yi Liu[1] · Jing Huang[1] · Hua Li[1]

Submitted: 17 June 2018 / in revised form: 28 October 2018 / Published online: 21 November 2018

Abstract There have been persistent challenges in thermal spraying of nanoparticles feedstock for making nanostructured coatings with desired mechanical strength. Here we report fabrication of nanostructured titania coatings by atmospheric plasma spraying of hollow titania spheres, and microstructures and photocatalytic activities of the coatings are examined. The hollow microspheres are ~ 50 μm in diameter and possess a mesoporous shell of 1-3 μm in thickness. The coatings show micro-nano hybrid structures with well-retained titania nanoparticles and agglomerated granules. High anatase content is achieved in the coatings, suggesting that constrained heating of the particles effectively prevents the transformation from anatase to rutile. The spherical characteristics of the organic materials in the feedstock powder play dominant roles in regulating the physicochemical characteristics of the coatings for photocatalytic performances. These results would provide insight into large-scale thermal spray fabrication of nanostructured coatings using appropriately designed hollow spherical powder.

Keywords hollow microspheres · nanostructured coatings · photocatalytic performances · plasma spray · titania nanoparticles

Introduction

Research efforts pertaining to photocatalysis have been booming for the applications of eliminating organic contaminants in water since it was first proposed by Fujishima and Honda in early 1970s (Ref 1). Photocatalytic oxidation is a viable and effective process, for it uses solar energy to drive the treatment and has clean reaction products (Ref 2-5). Titania has been used extensively for the last 40 years as an effective photocatalyst to destroy organic compounds and microorganisms, which is attributed to its chemical stability, high photoreactivity, long durability, nontoxicity, low cost, and repeatable usage without substantial loss of catalytic activity (Ref 6, 7). However, the use of titania particles usually bears additional centrifugation or microfiltration to separate the particles from the treated liquids (Ref 8). Moreover, the tendency of nanoparticles to agglomerate would greatly reduce their photocatalytic activity. To tackle these problems, immobilization of nanoparticles catalysts on various supports, such as glasses, silica, polymers, vesicles, and micelles (Ref 8, 9), has been attempted. In most cases, coating preparation of catalysts has been proven effective. Various techniques have been reported, including sol–gel method (Ref 10-12), physical vapor deposition (Ref 13-15), chemical vapor deposition (Ref 16-18), oxidation of Ti plate (Ref 19), dipping/sintering (Ref 20, 21), and thermal spray (Ref 22-24). Compared with other techniques, thermal spray appears to offer the possibility of large-scale fabrication of the active surfaces with a relatively high deposition rate (Ref 25).

Electronic supplementary material The online version of this article (https://doi.org/10.1007/s11666-018-0788-x) contains supplementary material, which is available to authorized users.

✉ Hua Li
lihua@nimte.ac.cn

[1] Key Laboratory of Marine Materials and Related Technologies, Zhejiang Key Laboratory of Marine Materials and Protective Technologies, Ningbo Institute of Materials Technology and Engineering, Chinese Academy of Sciences, Ningbo 315201, China

[2] Reliability Engineering Institute, National Engineering Research Center for Water Transport Safety, Wuhan University of Technology, Wuhan 430063, China

Thermal-sprayed photocatalytic TiO_2 coatings have been reported in recent years (Ref 22-24). Considering photocatalytic efficiency, the predominant presence of active anatase phase in titania coatings and small gain sizes are essential for favorable photocatalytic activity. Yet, the high temperature endured by the sprayed particles during thermal spraying process easily triggers undesired phase transformation of titania from anatase to rutile, which impairs the photocatalytic performances (Ref 23). Even though this transformation could be alleviated by an alternative technical route, suspension plasma spraying with titania feedstock suspensions (Ref 26), the as-sprayed nanostructured titania coatings are not as glamorous as expected for their inferior mechanical properties. The ease of abscission of titania nanoparticles or even peeling-off of the bulk coating would lower the efficacy of thermal spray approach and functional service life of the coatings. Meanwhile, the dispersing nanoparticles during thermal spray processing have negative impact on safety.

Developing new starting feedstock comprised of titania nanoparticles would be a solution for thermal spray construction of titania coatings with both sufficient mechanical strength and photocatalytic activity. In this study, hollow titania microspheres comprising titania nanoparticles were employed to deposit coatings by traditional atmospheric plasma spraying. The bound nature of the nanoparticles in the hollow sphere particles would appear to bring about alleviated health and safety hazard problems during thermal spraying. The hollow microspheres were prepared by suspension plasma spraying with titania nanoparticles, which has been discussed in detail in our previous work (Ref 27). The special hollow microspheric structures and the organic materials of the microspheres resulted in significantly retained anatase phase in the plasma-sprayed titania coatings. Excellent photocatalytic degradation of methylene blue was further revealed for the coatings.

Materials and Methods

Preparation of Titania Hollow Spheres

Commercial Degussa P25 powder (Evonik Degussa P25, 99.5%) was chosen as the raw material. The powder particles were $\sim$ 21 nm in diameter and comprised $\sim$ 80 wt.% anatase and $\sim$ 20 wt.% rutile. Suspension plasma spraying and spray-drying were conducted for preparing the agglomerated powder for the coating deposition. The experimental procedures for making hollow spheres have been reported previously (Ref 27).

Deposition of Titania Coatings

316L stainless steel plates with the dimensions of $30 \times 25 \times 2$ mm^3 were used as substrates. An APS-2000 K plasma spray system (Beijing Aeronautical Manufacturing Technology Research Institute, China) was employed to deposit the coatings with net powers of 12, 16 and 20 kW, respectively. Prior to the spraying, the substrates were surface grit-blasted using 60-mesh black fused alumina sand. Argon was used as the primary gas with the flow rate of 40 L/min. The auxiliary gas was hydrogen with a flow rate of 11 L/min. The powder feeding rate was 200 r/min, and the spray distance was 100 mm.

Characterization of the Powder and the Coatings

Phase compositions of the powders and the coatings were analyzed by x-ray diffraction (XRD, D8 Advance, Bruker AXS, Germany) with Cu K_α radiation operated at 40 kV and 40 mA. The goniometer was set at a scan rate of 0.02 °/s with the 2θ ranging from 10° to 90°. Quantification of the phases in the coatings was made by calculating the relative intensity of their major XRD peaks: $V_A = 8\times I_A/(8 \times I_A + 13 \times I_R) \times 100\%$ (Ref 28), where V_A is the volume fraction of anatase, and I_A and I_R are the XRD peak intensities of the (101) peak of anatase and the (110) peak of rutile, respectively. The data were recalculated into weight fraction using 3.78 g/cm^3 and 4.23 g/cm^3 as the densities of anatase and rutile, respectively. The crystallite size (d) was calculated by using the Debye–Scherrer formula: $d = k\lambda/(\beta \times \cos\theta)$, where k, λ, β, and θ represent the shape constant ($\sim$ 0.89), the x-ray wavelength (0.154056 nm), the half width of the diffraction peak (in radians), and Bragg angle, respectively. Microstructure of the coatings was characterized by field emission scanning electron microscopy (FESEM, FEI Quanta FEG S4800). Fourier transform infrared spectroscopy (FTIR, Nicolet 6700, Thermo Fisher Scientific, USA) was also used to characterize the chemistry of the samples. The infrared spectrum with a resolution of 4 cm^{-1} and the scan number of 8 were adopted with a spectral region from 400 to 4000 cm^{-1}. Surface roughness was examined by confocal laser scanning microscopy (CLSM, Zeiss LSM 700, Germany) equipped with ZEN 2012 software. Wettability of the coatings was assessed by measuring the contact angle of deionized distilled water droplets spreading on their surfaces using a contact angle measurement instrument (Dataphysics OCA20, Germany) at room temperature.

Assessment of Photocatalytic Performances

Photocatalytic activity of coatings was evaluated by degrading methylene blue (MB, Aladdin Reagent

Corporation, Shanghai, China). For MB degradation testing, a coating sample was immersed in Ø9 cm *Petri* culture dish containing 30 mL 5 ppm MB solution and then mechanical dispersion conducted by magnetic stirring for 1 h in dark to ensure adsorption/desorption equilibrium before irradiation. The solution was also continuously stirred by a magnetic stirrer throughout the experiment. Irradiation was made by a 15 W UV lamp (PHILIPS, TLD15 W BL) with the typical wavelength of 365 nm, and the distance between the UV light source and the sample was 15 cm. Variation at regular time intervals of MB concentration was analyzed by measuring absorption of MB at 664 nm using a UV–Vis spectrophotometer (Lambda 950, Perkin-Elmer, USA). The variations in MB concentration over irradiation time usually follow the Langmuir–Hinshelwood first-order kinetic equation, which is usually applied to low concentrations (Ref 27). According to the model, the equation, $\ln(C_0/C) = kt$, can be obtained. In this case, C is the MB concentration (ppm), C_0 is the MB initial concentration after residing in dark (ppm), t is the irradiation time (h), and k is the apparent rate constant representing photocatalytic degradation rate. The plot of $\ln(C_0/C)$ versus time yields a straight line and the slope refers to the apparent rate constant k.

Results and Discussion

Similar XRD peaks for the plasma-sprayed titania powder and the spray-dried titania powder were detected (Fig. 1A). The organic components were detected in the starting hollow titania spheres (Inset in Fig. 1A-1). From the IR spectra, the presence of the residual organic species (PVP/PEG in this case) in the hollow spheres are evidenced by the appearance of the peaks at 1273, 1370, 1440, and 1654 cm^{-1}, which are attributed to stretching vibrations of C-H, C-N, C-H, and C=O, respectively. The IR peaks at 2923 and 2852 cm^{-1} are assigned to C-H stretching vibrations of residual organics. Yet, no such IR peaks are seen for the spray-dried powder. Traces of XRD peaks for rutile are recognized in both the powder samples. Since the spray-drying temperature was $\sim$ 200 °C, which is much lower than the transformation temperature of titania (Ref 29), it is not surprising that no further transformation from anatase to rutile was detected in the spray-dried powder. It was already realized that the suspension plasma spray, the route used for preparing the titania hollow spheres (Ref 27), did not trigger obvious transformation of anatase to rutile. However, the plasma-sprayed and the spray-dried powder exhibits different morphologies (Fig. 1B and C). The size of the spray-dried particles is a little smaller than that of the suspension plasma-sprayed hollow spheres. The majority of powder particles fabricated by suspension plasma spray showed hollow structure. It is already clear that the hollow structure is mainly induced by rapid solvent evaporation, transfer of the titania nanoparticles from the inside to the outer surface, and inflation of internal steam and gas pressure (Ref 27). The hollow microspheres are $\sim$ 50 μm in diameter and have mesoporous shells (1-3 μm in thickness, which was statistically determined by a series of cross-sectional SEM images). The residual organic material is easily seen on the sphere surfaces (Fig. 1C-1) and distributed in the outer surface. To further evidence the presence of the organic binder in the hollow spheres, thermogravimetric analysis (TG) characterization was also conducted (Fig. S1). The TG curve of the hollow spheres can be divided into three parts, 50 $\sim$ 250 °C, 250 $\sim$ 350 °C and 350 $\sim$ 550 °C. In the first stage (50 $\sim$ 250 °C), the mass reduction is $\sim$ 3% due to the removal of adsorbed water. In the second stage (250 $\sim$ 350 °C) the mass reduction is $\sim$ 13% due to the removal of PEG with a decomposition temperature of $\sim$ 286 °C. In the third stage (350 $\sim$ 550 °C), the mass reduction is $\sim$ 15.5% due to the removal of PVP since the decomposition temperature of PVP is around 450 °C. These mass decreases are attributed to the decomposition of organic PEG and PVP in the hollow particles. It is very likely that the residual organic binder in the hollow spheres can be removed by heating at 550 °C. For the spray-dried powder, titania nanoparticles are seen and no organic material is obviously recognized (Fig. 1B-2 and C-2). In addition, cross section of the spray-dried particle shows solid structure (the inset in Fig. 1B-2).

After the coating deposition, phase transformation is observed for titania (Fig. 2), and it is indicated by the intensified XRD peaks for rutile. Small net power of the plasma spray gave rise to less transformation from anatase to rutile (12 kW and 16 kW versus 20 kW). For the lower spray power, more than 30 wt.% anatase is remained in coatings made from the hollow titania spheres (Fig. 2A and B). The calculated results are listed in Table 1. It is found that both the anatase content and crystallite size are remarkably influenced by the characteristics of the starting powder and the plasma spray power.

As the comparison, the coatings made from the spray-dried titania powder show severe transformation of anatase to rutile, as indicated by significantly weakened XRD peaks for anatase (Fig. 2D and F). In addition, the spray power of 12 kW already led to some undesired phase transformation, resulting in the composition of $\sim$ 3.04 wt.% for anatase and $\sim$ 96.96 wt.% for rutile in the coating. The spray power of 16 kW already resulted in growth of grains. These results suggest that the morphological features and the organics existing in the starting feedstock particles play critical roles in regulating the chemistry of the coatings. It is notable that the hollow

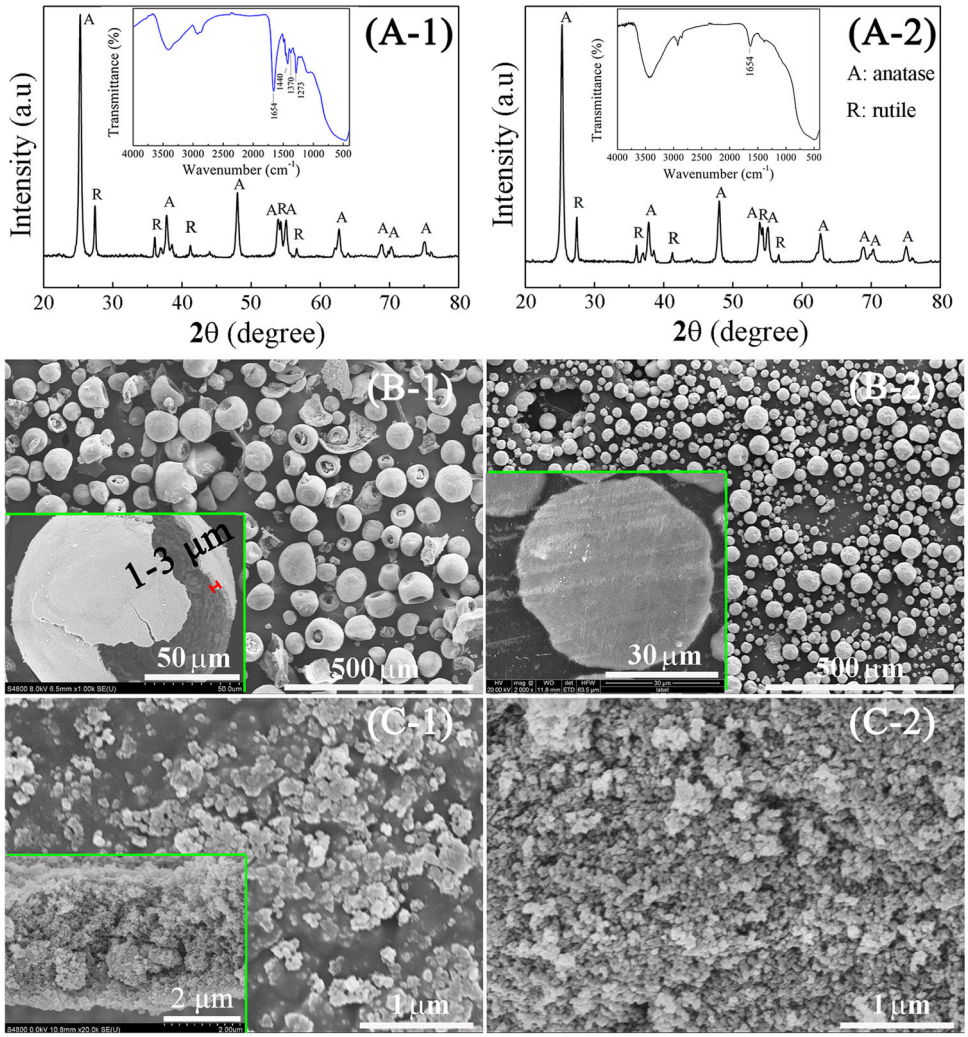

Fig. 1 Characteristics of the starting powder, (A-1) XRD pattern of the hollow titania spheres (the inset is the FTIR spectrum of the powder), (A-2) XRD pattern of the spray-dried titania powder (the inset is the FTIR spectrum of the powder), (B-1) FESEM picture of the hollow titania spheres (the inset is the enlarged view of a crushed particle), (B-2) FESEM picture of the spray-dried titania powder (the inset is the cross-sectional view of a particle), (C-1) enlarged SEM view of the surface of the hollow titania spheres (the inset is the cross-sectional view of mesoporous shell of a hollow titania sphere), and (C-2) enlarged SEM view of the surface of the spray-dried titania powder

spherical structure and the organic components in the particle shell facilitate retention of anatase. It is likely that the organic components existing in the shells of the hollow spheres slow down the heat transfer during the in-flight stage of the particles. As already shown in Fig. 1(C-1) and TG analyses (Fig. S1), pronounced presence of residual organics in the shells of the hollow spheres were revealed. The residual organic components of the hollow titania spheres could absorb plenty of heat to avoid overheating of the titania nanoparticles and consequently constrain anatase–rutile transformation and slow down the heat transfer to inner surface of the shells of the spheres. In addition, the porous shell and the interior hollow geometry of the hollow spheres could slow down the heat transfer, since the hollow spheres have much lower thermal conductivity than bulk titania. Our ongoing efforts are devoted to continuously improving the retention of anatase phase using the hollow powder.

Microstructural characterization further revealed well-retained titania nanoparticles in the coatings made from the hollow spheres (Fig. 3). For the coatings fabricated using the spray powers of 12 and 16 kW, granules or block aggregates are observed on their top surfaces (Fig. 3A and B). Close view of the surface of the coating deposited with 12 kW net power clearly shows the nanoparticles with particle size of 25 ∼ 45 nm (Fig. 3A-2). Size of the nanoparticles was examined by using *ImageJ* software. Similar topographical structural feature is also recognized for the coating made with 16 kW net power; however, the particle size is a little bigger (∼ 40 nm, Fig. 3B-2). When the spray power further increased to 20 kW, no more nanoparticles are seen for the coating (Fig. 3C-1, C-2). This result is not surprising as the nanoparticles existing in the starting hollow spheres encountered severe heating and consequently deteriorated anatase–rutile transformation. In that case, complete melting of the hollow spheres easily results in remarkable grain growth. For the coatings made from the spray-dried powder, however, typical micron-sized structures are seen in the coatings deposited using the spray power of 12 kW and 16 kW, showing a well melting

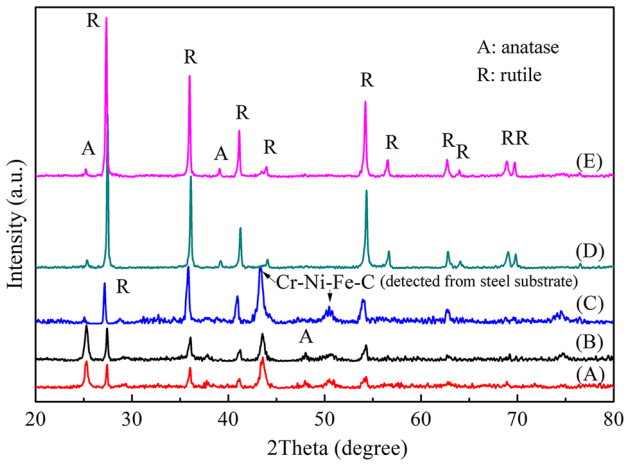

Fig. 2 XRD curves of the coating made from the hollow spheres with the spray power of 12 kW (A), the coating made from the hollow spheres with the spray power of 16 kW (B), the coating made from the hollow spheres with the spray power of 20 kW (C), the coating made from the spray-dried powder with the spray power of 12 kW (D), and the coating made from the spray-dried powder with the spray power of 16 kW (E)

state of the particles and typical flaws (Fig. 3D and E). Nanoparticles are not seen, which were presumably fused during the high-temperature spraying process and merged into bumps in the size of microns or submicrons. Interconnections of the starting titania nanoparticles are clearly seen as the grain boundaries (Fig. 3D-2 and E-2). These structural features are consistent with the XRD results that the coatings made from the spray-dried powder already lost the nanostructural features and were predominantly rutile. In addition, for both the coatings, dense cross-sectional microstructure was revealed (Fig. S2). The topographical morphology of the coatings plays a role in deciding their photocatalytic performances.

Their surface roughness and wettability were also investigated. High roughness would facilitate the photocatalytic performances of the coatings, due to increased contact area of MB solution (Ref 30). The surface roughness values, arithmetical mean deviation of the assessed profile (R_{sa}), maximum peak height of profile (R_{sz}) and surface kurtosis (R_{sku}), were measured by CLSM and analyzed by ZEN 2012 software. The R_{sa} values of all the coatings made from the hollow spheres are relatively smaller than those of the coatings made from the spray-dried powder (Fig. 4), which can be simply explained by differences in grain sizes and topographical morphologies of the coatings. In addition, it is noted that the higher spray power, 16 versus 12 kW, triggered slightly increased R_{sa} values, 5.08 μm versus 4.31 μm, for the coatings made from the hollow spheres. This could be explained by the production of enlarged grains. However, further increased spray power to 20 kW leads to a decreased R_{sa} value, 4.38 μm versus 5.08 μm, which could be explained by the complete melting of the titania nanoparticles. For the coatings made from the spray-dried powder, an unusual phenomenon is seen. The R_{sa} value decreases with increased spray power (5.03 versus 5.56 μm), while R_{sz} value increases with increased spray power (50.12 μm versus 45.22 μm) and R_{sku} value also increases (3.49 versus 3.35).

The water contact angles are 46°, 32°, 0°, 93°, 137° for the coatings made from the hollow spheres at 12 kW, the hollow spheres at 16 kW, the hollow spheres at 20 kW, the spray-dried powder at 12 kW, and the spray-dried powder at 16 kW, respectively. The hydrophilic nature of the coatings made from hollow spheres is predominately attributed to the hydrophilic characteristic of TiO_2 nanoparticles. The superhydrophilicity of the coating

Table 1 Quantification of the phases in the coatings and calculated crystallite sizes

	Phase composition		Crystallite size (nm)	
	Anatase, wt.%	Rutile, wt.%	Crystallite size of anatase, nm	Crystallite size of rutile, nm
P25(a)	~ 74.12	~ 25.88	~ 22.93	~ 39.34
HS	~ 71.33	~ 28.67	~ 24.07	~ 42.76
SDP	~ 73.43	~ 26.57	~ 23.05	~ 42.34
A	~ 38.53	~ 61.47	~ 24.47	~ 44.69
B	~ 37.41	~ 62.59	~ 22.74	~ 42.35
C	~ 6.45	~ 93.55	~ 34.69	~ 47.98
D	~ 3.04	~ 96.96	~ 22.74	~ 42.34
E	~ 2.10	~ 97.90	~ 87.80	~ 56.38

(a) The data were calculated by XRD spectra of P25, which was a little different from the commercial data

HS, the hollow spheres; SDP, the spray-dried powder; A, the coating made from the hollow spheres with the spray power of 12 kW; B, the coating made from the hollow spheres with the spray power of 16 kW; C, the coating made from the hollow spheres with the spray power of 20 kW; D, the coating made from the spray-dried powder with the spray power of 12 kW; E, the coating made from the spray-dried powder with the spray power of 16 kW

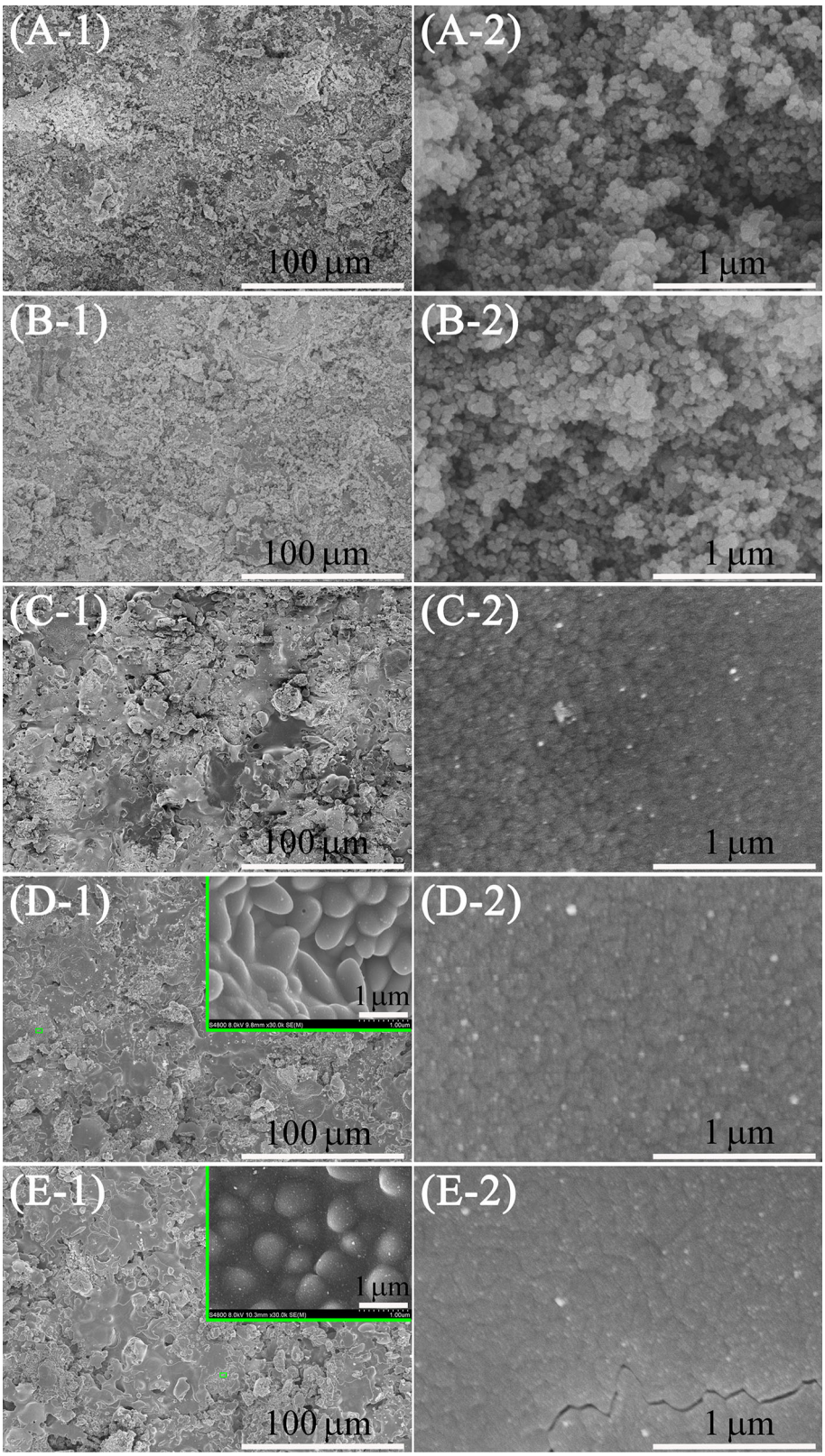

Fig. 3 Typical SEM images of the as-sprayed coatings showing their distinctive microstructures, (A-1) and (A-2): the coating made from the hollow spheres with the spray power of 12 kW, (B-1) and (B-2): the coating made from the hollow spheres with the spray power of 16 kW, (C-1) and (C-2): the coating made from the hollow spheres with the spray power of 20 kW, (D-1) and (D-2): the coating made from the spray-dried powder with the spray power of 12 kW, and (E-1) and (E-2): the coating made from the spray-dried powder with the spray power of 16 kW. (-2 are enlarged views of -1, and the insets in (D-1) and (E-1) are further enlarged views of selected areas)

deposited using 20 kW spray power suggest contributions by both the nanoparticles and the significantly intensified interconnections between adjacent titania nanoparticles (Fig. 3C). In contrast, the coatings made from spray-dried powder are hydrophobic, and their hydrophobicity is enhanced with increased spray power. This could be

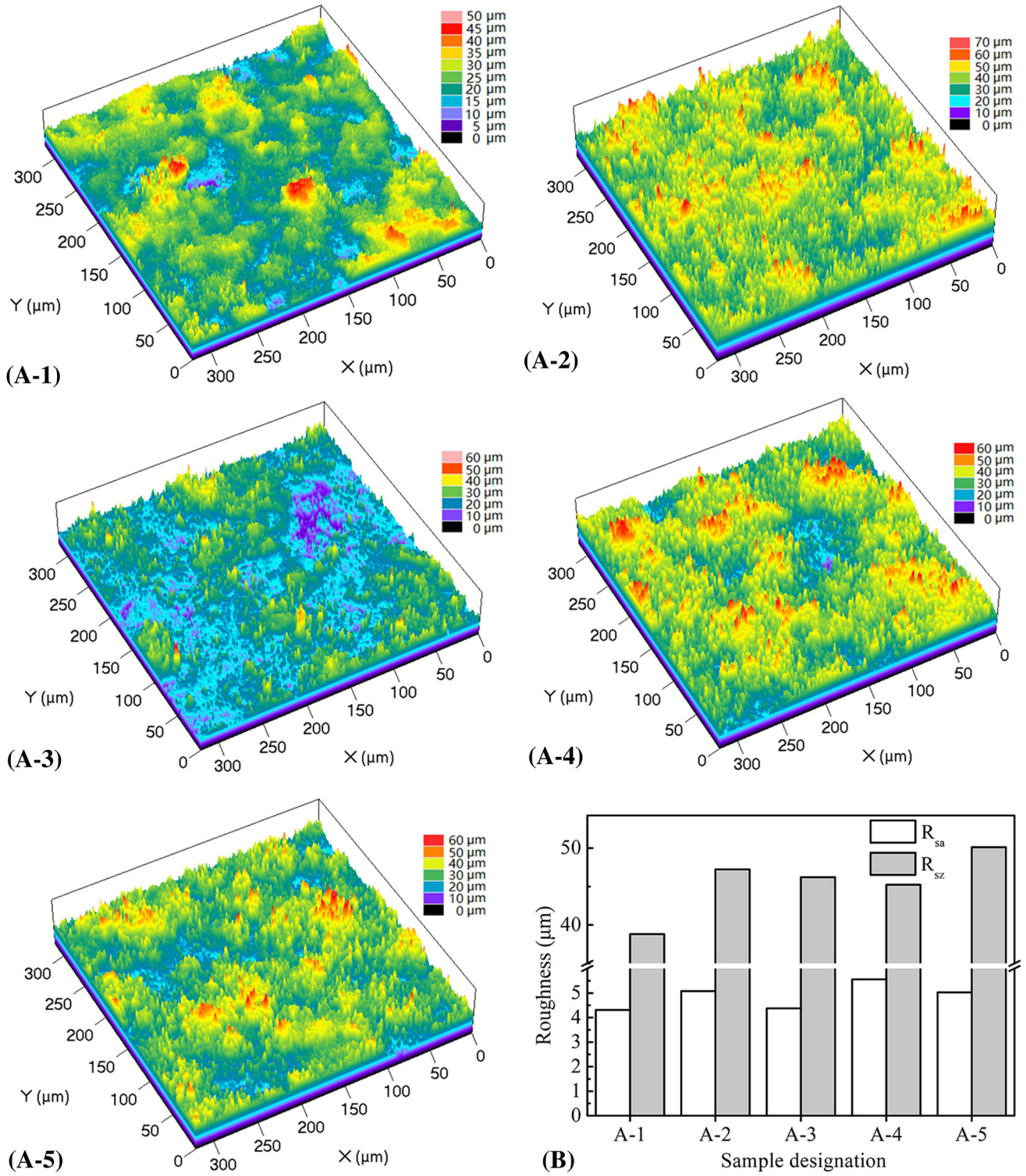

Fig. 4 A: CLSM images showing the surfaces of the titania coatings made from the hollow titania sphere and the spray-dried powder (A-1: the coating made from the hollow spheres with the spray power of 12 kW, A-2: the coating made from the hollow spheres with the spray power of 16 kW, A-3: the coating made from the hollow spheres with the spray power of 20 kW, A-4: the coating made from the spray-dried powder with the spray power of 12 kW, and A-5: the coating made from the spray-dried powder with the spray power of 16 kW), and B: Roughness of the coatings

attributed to their hybrid micro-/nano-surface structures (insets in Fig. 3D-1 and E-1). Wettability is also known to play a role in tailoring photocatalytic performance; hydrophilicity usually promotes the photocatalytic activity of TiO_2 (Ref 31).

Photocatalytic activities of the coatings were assessed by degrading MB under UV irradiation. Variation in the photocatalytic degradation of MB is shown in Fig. 5 (C_{-1} is the MB concentration measured 1 h before the illumination and C_0 is the MB concentration measured immediately before the illumination). It is clear that the degradation was enhanced by elongated UV exposure, and the MB decomposition rate decreases with the increased reaction time. When no coating participates in the MB degradation, slight degradation ($\sim$ 6.6%) after 5.5 h of UV irradiation could be neglected. Notably, the coatings made from the hollow titania spheres using the spray powers of 12, 16, and 20 kW exhibit the photocatalytic performances of $\sim$ 66.8, $\sim$ 76.0, and $\sim$ 24.4% degradation of MB, respectively. The photocatalytic performance of the coating made from the hollow spheres with the spray power of 16 kW is better than that of the coating made from the hollow spheres with the spray power of 12 kW. This is likely attributed to the differences in surface roughness and wettability. The coatings made from the spray-dried titania powder using the spray power of 12 and 16 kW showed poor photocatalytic activities ($\sim$ 19.6, and $\sim$ 27.4% degradation of MB, respectively), predominately because of their low anatase content and their micro-sized structures. Surprisingly, the photocatalytic activity of the coating sprayed with the spray power of 16 kW is slightly better than that of the coating sprayed with the spray power of 12 kW. In this case, R_{sz} plays important roles. These changes in the observed different photocatalytic activities are consistent with surface roughness.

Variations in $\ln(C_0/C)$ with irradiation time of coating samples are acquired (Fig. 5C). The coating made from the hollow titania spheres with the spray power of 16 kW possesses the best photocatalytic performance, showing a k value of 0.221 h^{-1} which is almost about sixfolds of the coating made from the spray-dried powder with the same spray power (0.038 h^{-1}). These photocatalytic performances of the coatings made from the hollow spheres are much better than those made from the spray-dried powder. These results agree well with both the chemistry and morphological features of the coatings.

Phase composition, surface morphologies, and wettability are significant variables that influence the photocatalytic performance of thermal-sprayed titania coating (Ref 8, 22, 25, 32-34). Synergistic effect of anatase and rutile was also reported (Ref 35). The photoactivity of coatings and their physicochemical properties, including phase composition, roughness, and wettability are listed in

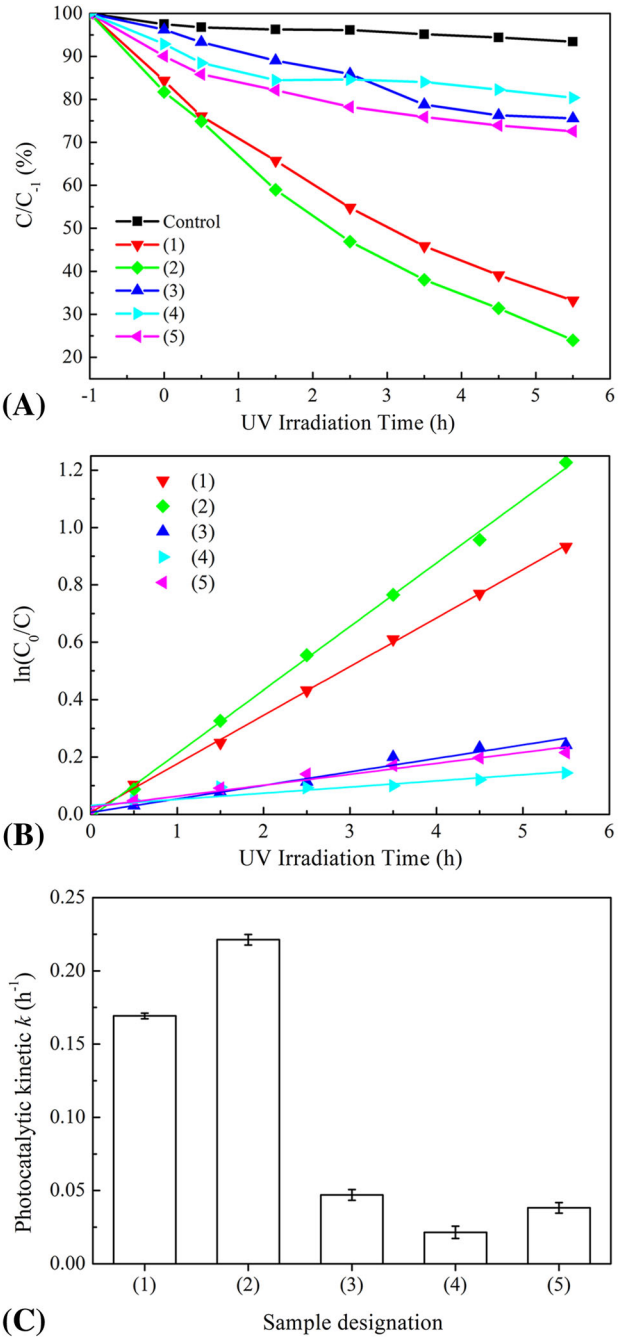

Fig. 5 Photocatalytic activities of the coatings tested under UV irradiation, A: variation of MB concentration vs. UV illumination time, B: $\ln(C_0/C)$ vs. UV irradiation time in the presence of the coatings prepared under different spray power, and C: photocatalytic kinetic k values calculated from the curves shown in B ((1): the coating made from the hollow spheres with the spray power of 12 kW, (2): the coating made from the hollow spheres with the spray power of 16 kW, (3): the coating made from the hollow spheres with the spray power of 20 kW, (4): the coating made from the spray-dried powder with the spray power of 12 kW, and (5): the coating made from the spray-dried powder with the spray power of 16 kW)

Table 2 Photoactivity of the coatings and their phase composition, surface roughness and wettability

Coatings	Photocatalytic activities		Phase composition	Roughness			Wettability
	Degradation	Photocatalytic kinetic, h^{-1}	Anatase, wt.%	R_{sa}, μm	R_{sz}, μm	R_{sku}	Contact angle
A	~ 66.8%	0.169	~ 38.53	4.31	38.82	3.53	46°
B	~ 76.0%	0.221	~ 37.41	5.08	47.23	3.27	32°
C	~ 24.4%	0.047	~ 6.45	4.38	46.21	3.48	0°
D	~ 19.6%	0.021	~ 3.04	5.56	45.22	3.35	93°
E	~ 27.4%	0.038	~ 2.10	5.03	50.12	3.49	137°

A, the coating made from the hollow spheres with the spray power of 12 kW; B, the coating made from the hollow spheres with the spray power of 16 kW; C, the coating made from the hollow spheres with the spray power of 20 kW; D, the coating made from the spray-dried powder with the spray power of 12 kW; E, the coating made from the spray-dried powder with the spray power of 16 kW

Table 2. Briefly, more active phase, the anatase phase in this case, means more active sites to induce photocatalytic reactions. Besides, adsorption capacity impacts the photocatalytic activity, and the adsorption is closely related to surface roughness and wettability. The use of hollow titania spheres clearly weakened the heating of powder for consequent phase transformation and grain growth. The coating prepared using the hollow spheres and 16 kW spray power showed the best photodegradation performance, and this phenomenon agreed perfectly with synergistic effects brought about by the anatase content, surface roughness, and hydrophilicity. It is still a great challenge to clarify the photocatalytic trends in the spraying process since these impact factors, such as phase composition, crystal size surface morphologies, and wettability, are difficult to independent control in the spraying process. The results give certain insight into developing effective ways of utilizing hollow microspheres to fabricate surface coatings for desired microstructures and functions.

Conclusions

Both hollow titania spheres and spray-dried titania powder in micron sizes were used for plasma spray. The starting feedstock powders both had the titania nanoparticles as the sole component. The hollow spherical structure and the presence of organic materials in the starting powder facilitated retention of the titania nanoparticles in the as-sprayed coatings, and preliminary attempts in optimizing spray parameters showed the net power of 16 kW to be appropriate for producing coating with favorable photocatalytic performances. The relatively solid spray-dried powder particles encountered effective heating during the spraying process, which resulted in significant grain growth and severe phase transformation from anatase to rutile. The tailorable nanostructures yielded insight into large-scale thermal spray fabrication of nanostructured functional coatings using nanoparticles as the starting feedstock.

Acknowledgments This work was supported by Key Research and Development Program of Zhejiang Province (2017C01003), National Natural Science Foundation of China (31500772 and 41476064), International Scientific and Technological Cooperation Project of Ningbo (2016D10012), China Postdoctoral Science Foundation (2017M622542), and Hubei Postdoctoral Sustentation Foundation (G22).

References

1. A. Fujishima, Electrochemical Photolysis of Water at a Semiconductor Electrode, *Nature*, 1972, **238**, p 37-38
2. C. Dominguez, J. Garcıa, M. Pedraz, A. Torres, and M. Galan, Photocatalytic Oxidation of Organic Pollutants in Water, *Catal. Today*, 1998, **40**(1), p 85-101
3. D.M. Blake, P.C. Maness, Z. Huang, E.J. Wolfrum, J. Huang, and W.A. Jacoby, Application of the Photocatalytic Chemistry of Titanium Dioxide to Disinfection and the Killing of Cancer Cells, *Separ. Purif. Methods*, 1999, **28**(1), p 1-50
4. R.K. Nath, M. Zain, and A.A.H. Kadhum, Photocatalysis-a Novel Approach for Solving Various Environmental and Disinfection Problems: A Brief Review, *J. Appl. Sci. Res.*, 2012, **8**(8), p 4147-4155
5. O.K. Dalrymple, E. Stefanakos, M.A. Trotz, and D.Y. Goswami, A Review of the Mechanisms and Modeling of Photocatalytic Disinfection, *Appl. Catal. B Environ.*, 2010, **98**(1), p 27-38
6. K. Nakata and A. Fujishima, TiO_2 Photocatalysis: Design and Applications, *J. Photochem. Photobiol. C*, 2012, **13**(3), p 169-189
7. J. Gamage and Z. Zhang, Applications of Photocatalytic Disinfection, *Int. J. Photoenergy*, 2010, **4**, p 5. https://doi.org/10.1155/2010/764870
8. F. Ye and A. Ohmori, The Photocatalytic Activity and Photo-Absorption of Plasma Sprayed TiO_2-Fe_3O_4 Binary Oxide Coatings, *Surf. Coat. Technol.*, 2002, **160**(1), p 62-67
9. Y.S. Choi and B.W. Kim, Photocatalytic Disinfection of *E. coli* in a UV/TiO_2-Immobilised Optical-Fibre Reactor, *J. Chem. Technol. Biotechnol.*, 2000, **75**(12), p 1145-1150
10. H. Choi, E. Stathatos, and D.D. Dionysiou, Photocatalytic TiO_2 Films and Membranes for the Development of Efficient Wastewater Treatment and Reuse Systems, *Desalination*, 2007, **202**(1), p 199-206

11. J.G. Yu, X.J. Zhao, J.C. Du, and W.M. Chen, Preparation, Microstructure and Photocatalytic Activity of the Porous TiO_2 Anatase Coating by sol–gel Processing, *J. Sol Gel Sci. Technol.*, 2000, **17**(2), p 163-171
12. K. Yoshida, K. Okamura, K. Itoh, and M. Murabayashi, Photocatalytic Degradation of Chlorinated Compounds in Water. Effect of the Number of the Repeated Dip-Coating for the TiO_2 Thin-Film on the Degradation of Tce, *Denki Kagaku*, 1998, **66**(2), p 171-175
13. P. Zeman and S. Takabayashi, Nano-scaled Photocatalytic TiO_2 Thin Films Prepared by Magnetron Sputtering, *Thin Solid Films*, 2003, **433**(1-2), p 57-62
14. M. Yamagishi, S. Kuriki, P.K. Song, and Y. Shigesato, Thin Film TiO_2 Photocatalyst Deposited by Reactive Magnetron Sputtering, *Thin Solid Films*, 2003, **442**(1-2), p 227-231
15. S. Takeda, S. Suzuki, H. Odaka, and H. Hosono, Photocatalytic TiO_2 Thin Film Deposited onto Glass by DC Magnetron Sputtering, *Thin Solid Films*, 2001, **392**(2), p 338-344
16. H. Yoshiki and T. Mitsui, TiO_2 Thin Film Coating on a Capillary Inner Surface Using Atmospheric-Pressure Microplasma, *Surf. Coat. Technol.*, 2008, **202**(22-23), p 5266-5270
17. A. Mills, N. Elliott, I.P. Parkin, S.A. O'Neill, and R.J. Clark, Novel TiO_2 CVD Films for Semiconductor Photocatalysis, *J. Photochem. Photobiol. A*, 2002, **151**(1-3), p 171-179
18. B.H. Kim, J.Y. Lee, Y.H. Choa, M. Higuchi, and N. Mizutani, Preparation of TiO_2 Thin Film by Liquid Sprayed Mist CVD Method, *Mater. Sci. Eng. B*, 2004, **107**(3), p 289-294
19. Y. Wu, M. Long, W. Cai, S. Dai, C. Chen, D. Wu, and J. Bai, Preparation of Photocatalytic Anatase Nanowire Films by In Situ Oxidation of Titanium Plate, *Nanotechnology*, 2009, **20**(18), p 185703
20. K. Sunada, Y. Kikuchi, K. Hashimoto, and A. Fujishima, Bactericidal and Detoxification Effects of TiO_2 Thin Film Photocatalysts, *Environ. Sci. Technol.*, 1998, **32**(5), p 726-728
21. Y. Takahashi and Y. Matsuoka, Dip-Coating of TiO_2 Films Using a Sol Derived from $Ti(O\text{-}i\text{-}Pr)_4$-Diethanolamine-$H_2O$-i-Proh System, *J. Mater. Sci.*, 1988, **23**(6), p 2259-2266
22. Z. Yi, J. Liu, W. Wei, J. Wang, and S.W. Lee, Photocatalytic performance and Microstructure of Thermal-Sprayed Nanostructured TiO_2 Coatings, *Ceram. Int.*, 2008, **34**(2), p 351-357
23. C. Lee, H. Choi, C. Lee, and H. Kim, Photocatalytic Properties of Nano-structured TiO_2 Plasma Sprayed Coating, *Surf. Coat. Technol.*, 2003, **173**(2), p 192-200
24. T. Kanazawa and A. Ohmori, Behavior of TiO_2 Coating Formation on Pet Plate by Plasma Spraying and Evaluation of Coating's Photocatalytic Activity, *Surf. Coat. Technol.*, 2005, **197**(1), p 45-50
25. F.L. Toma, L.M. Berger, C.C. Stahr, T. Naumann, and S. Langner, Microstructures and Functional Properties of Suspension-Sprayed Al_2O_3 and TiO_2 Coatings: An Overview, *J. Therm. Spray Technol.*, 2010, **19**(1-2), p 262-274
26. F.L. Toma, G. Bertrand, D. Klein, C. Coddet, and C. Meunier, Nanostructured Photocatalytic Titania Coatings Formed by Suspension Plasma Spraying, *J. Therm. Spray Technol.*, 2006, **15**(4), p 587-592
27. K. Ren, Y. Liu, X. He, and H. Li, Suspension Plasma Spray Fabrication of Nanocrystalline Titania Hollow Microspheres for Photocatalytic Applications, *J. Therm. Spray Technol.*, 2015, **24**(7), p 1213-1220
28. Z. Pala, E. Shaw, J.W. Murray, N. Senin, and T. Hussain, Suspension High Velocity Oxy-Fuel Spraying of TiO_2: A Quantitative Approach to Phase Composition, *J. Eur. Ceram. Soc.*, 2017, **37**(2), p 801-810
29. D.A. Hanaor and C.C. Sorrell, Review of the Anatase to Rutile Phase Transformation, *J. Mater. Sci.*, 2011, **46**(4), p 855-874
30. P. Ctibor, Z. Pala, V. Stengl, and R. Musalek, Photocatalytic Activity of Visible-Light-Active Iron-Doped Coatings Prepared by Plasma Spraying, *Ceram. Int.*, 2014, **40**(1), p 2365-2372
31. S. Wang, K.K. Meng, L. Zhao, Q. Jiang, and J.S. Lian, Superhydrophilic Cu-Doped TiO_2 Thin Film for Solar-Driven Photocatalysis, *Ceram. Int.*, 2014, **40**(4), p 5107-5110
32. C. Zhang, U. Chaudhary, S. Das, A. Godavarty, and A. Agarwal, Effect of Porosity on Photocatalytic Activity of Plasma-Sprayed TiO_2 Coating, *J. Therm. Spray Technol.*, 2013, **22**(7), p 1193-1200
33. G.J. Yang, C.J. Li, Y.Y. Wang, and C.X. Li, Dominant Microstructural Feature Over Photocatalytic Activity of High Velocity Oxy-Fuel Sprayed TiO_2 Coating, *Surf. Coat. Technol.*, 2007, **202**(1), p 63-68
34. G.J. Yang, C.J. Li, S.Q. Fan, Y.Y. Wang, and C.X. Li, Influence of Annealing on Photocatalytic Performance and Adhesion of Vacuum Cold-Sprayed Nanostructured TiO_2 Coating, *J. Therm. Spray Technol.*, 2007, **16**(5-6), p 873-880
35. A.J. Gardecka, C. Bishop, D. Lee, S. Corby, I.P. Parkin, A. Kafizas, and S. Krumdieck, High Efficiency Water Splitting photoanodes Composed of Nano-structured Anatase-Rutile TiO_2 Heterojunctions by Pulsed-Pressure MOCVD, *Appl. Catal. B Environ.*, 2018, **224**, p 904-911